JOURNAL OF GEOPHYSICAL RESEARCH, VOL. 103, NO. D10, PAGES 11,341–11,353, MAY 27, 1998

# A cumulus parameterization with multiple cloud base levels

Ping Ding and David A. Randall

Department of Atmospheric Science, Colorado State University, Fort Collins

**Abstract.** We have generalized the Arakawa-Schubert cumulus parameterization to allow multiple cloud-base levels. A spectrum of cloud-top levels is allowed for each cloud-base level. We use a linear (rather than exponential) mass flux profile, because this greatly simplifies the determination of the entrainment rate and reduces the computational requirements of the parameterization. Cloud-top entrainment is included. The linear mass flux profile and the multiple cloud bases are separately tested in a general circulation model. Results show that the linear mass flux profile tends to lead to smoother precipitation distribution with a decrease in the depth and intensity of deep convection and that cumuli with cloud bases above the boundary layer tend to occur at night over land.

## 1. Introduction

A large fraction of all cumulus clouds have their bases at or near the top of the planetary boundary layer (PBL), and their updrafts draw air out of the PBL. As discussed below, however, both observations and numerical experiments suggest that cumulus updrafts sometimes originate well above the PBL.

A literature search has revealed surprisingly few papers on the subject of convection with elevated cloud bases, but there are some. *Warner et al.* [1980] analyzed a cloud cluster that occurred on September 18, 1974, during the GARP (Global Atmospheric Research Program) Atlantic Tropical Experiment (GATE). Cloud coverage over the aircraft box approached 50%, and cumulus towers were accompanied by altostratus, altocumulus, and cirrus clouds. They used aircraft, radar, satellite, and ship data to construct cloud maps, which show that many of the clouds had high bases; for example, one cumulonimbus cloud had a base slanting from 5 to 8 km. The cloud tops reached 13 km. Warner et al. concluded that such high-based convective clouds are symptomatic of convective instability released by uplift from below. Cloudiness during GATE was also studied by *Holle et al.* [1979], using hourly daytime whole-sky photographs taken aboard four U.S. ships. Clouds with bases higher than 2 km were defined as upper clouds. The average total cloud cover was 77%, and 41% of these were upper clouds.

Elsewhere in the tropics, *Warner and Grumm* [1984] used a variety of observations, including cloud photographs from aircraft, to study cloud distributions associated with a monsoon depression on July 7, 1979, in the Bay of Bengal. They found a dense overcast based at about 7.5 km above sea level, with contiguous cumuli.

Turning to middle latitudes, *Colman* [1983] studied an intense and persistent outbreak of elevated convection, beginning over northeast Texas on March 5, 1982, and continuing into March 6. Colman's analysis indicated that at the midlevels the convective line was organized ahead of a cyclonic circulation center. Temperature and moisture advection generated convective instability aloft. Meanwhile, strong frontogenesis occurred at 850 mbar, and the associated frontal circulation apparently triggered the convection. In this type of convection, no convective updraft air comes directly from the PBL.

Modeling studies also suggest the possible importance of convection starting above the PBL. For example, *Randall et al.* [1989] studied interactions among radiation, convection, and large-scale dynamics by using a general circulation model (GCM). In their study the penetrative cumulus convection originating in the PBL was represented through the cumulus parameterization of *Arakawa and Schubert* [1974, hereinafter referred to as AS], which they called "CUP." Manabe's moist convective adjustment parameterization, called "MSTADJ," was used as a supplementary parameterization for moist convection which originates above the PBL; this procedure was devised by the modeling group at UCLA, during the 1970s, and is described by *Suarez et al.* [1983]. (We emphasize that MSTADJ is used only to represent convection that originates above the PBL so that it does not duplicate any part of what CUP does.) *Randall et al.* [1989] reported that MSTADJ was very active in their simulations. Here we show similar results from the current Colorado State University (CSU) GCM, which is descended from the UCLA GCM and is described further later in this paper. Figure 1 shows the frequency of occurrence (hereinafter referred to as "incidence") of penetrative cumulus convection and moist convective adjustment, in a run with the current CSU GCM, for January and July. MSTADJ occurs as frequently as CUP, even in the tropics, in both January and July.

The studies discussed above strongly suggest that a cumulus parameterization should allow the possibility of convection originating at any and all possible levels. The ~~m~~ain purpose of this paper is to report the development of such a parameterization, based on the approach of AS.

As summarized in Table 1, some existing parameterizations do allow convection to originate at any level. Very few of these allow penetrative convection from multiple levels, however. In addition, the literature contains very little information about model-simulated convective activity that originates aloft.

Adding multiple cloud-base levels obviously increases the complexity and computational cost of a parameterization and would have been prohibitively difficult in the case of the already-complex AS parameterization had we not made major simplifications of the approach taken by AS and *Lord et al.* [1982]. We viewed simplification of the AS parameterization as a necessary preliminary step and approached it in two separate ways.

The first approach was adoption of the prognostic closure



Paper number 98JD00346.
0148-0227/98/98JD-00346$09.00

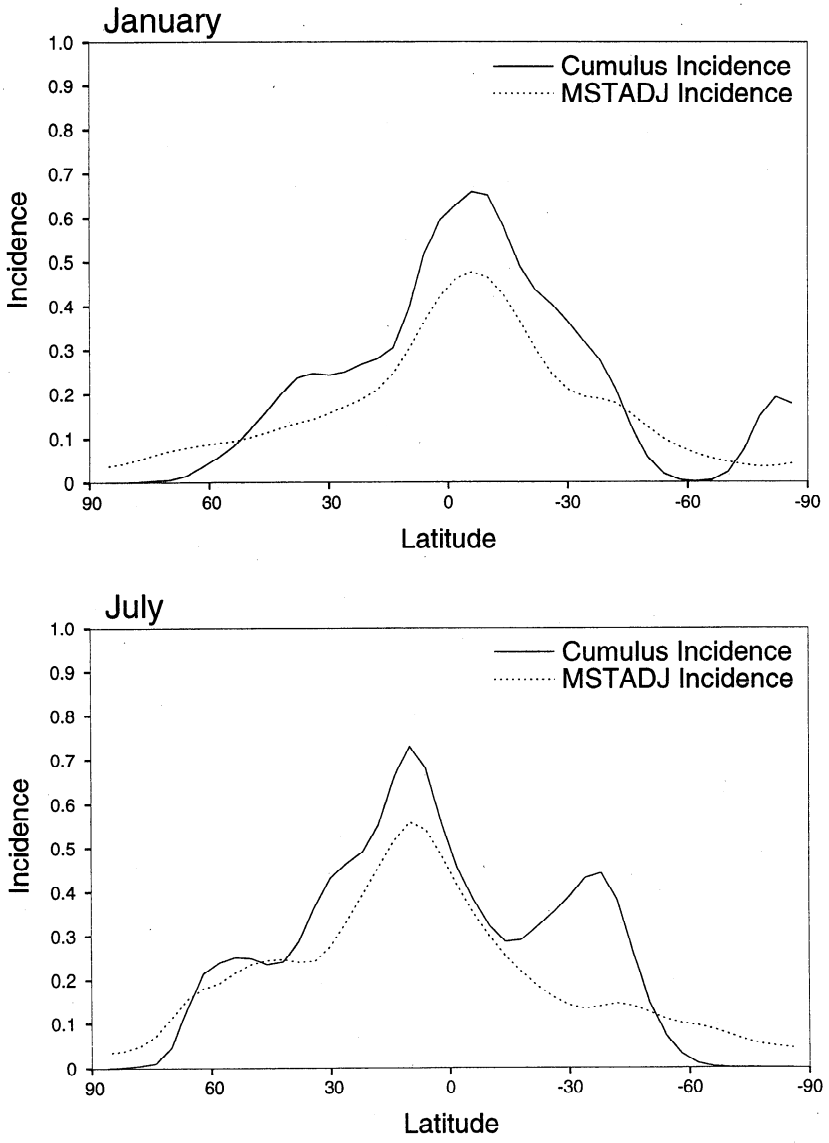


**Figure 1.** Zonally averaged CUP and MSTADJ incidence for January and July.

developed by *Randall and Pan* [1993] and *Pan and Randall* [1997]. The prognostic closure eliminates the need to solve the integral equation for the cloud-base mass flux [AS; *Lord et al.*, 1982], resulting in a drastic simplification of the parameterization as well as a doubling of its computational speed.

The second approach to simplification, which is discussed in this paper, is to replace the exponential mass flux profile of AS with a linear mass flux profile as proposed by *Moorthi and Suarez* [1992]. As explained later, the linear mass flux profile allows computation of the entrainment rate for each cloud type through solution of a simple linear equation, whereas with the exponential profile, the fractional entrainment rate must be determined through a complex and expensive iteration. The introduction of the linear mass flux profile leads to a further threefold reduction in the computational requirements of the cumulus parameterization.

Following these two simplifying changes, we generalized the cumulus parameterization to allow multiple cloud bases and performed further tests with the CSU GCM.

In summary, the main issues addressed by this paper are as follows:

1. What is the role of cumuli originating aloft (hereinafter COA) in the general circulation of the atmosphere?
2. To what extent is COA penetrative?
3. How can we include COA in the framework of the Arakawa-Schubert parameterization?
4. What are the effects of the linear mass flux profile on the results produced by the parameterization?

An outline of the paper is as follows: Section 2 describes the linear mass flux profile. Section 3 explains the implementation of multiple cloud-base levels. Section 4 provides a brief description of the CSU GCM. We then report the results of tests, first of the linear mass flux profile alone in section 5 and then of the effects of multiple cloud-base levels in section 6. A summary and conclusions are given in section 7.

## 2. Linear Mass Flux Profile

The fractional entrainment rate $\lambda$ is defined by

$$\frac{\partial \eta(z, \lambda)}{\partial z} \equiv \lambda \eta(z, \lambda). \tag{1}$$

**Table 1.** List of Some Cumulus Parameterizations and Their Assumptions, If Any, About the Cloud-Base Level

| Parameterization | Reference | Allowed Cloud-Base Levels |
|---|---|---|
| Moist convective adjustment | *Manabe et al.* [1965] | anywhere; convection does not penetrate |
| Kuo | *Kuo* [1965, 1974], *Anthes* [1977], *Raymond and Emanuel* [1993] | PBL only |
| Arakawa-Schubert | *Arakawa and Schubert* [1974] | PBL only; in some applications of the Arakawa-Schubert parameterization, moist convective adjustment has been used to separately parameterize convection originating above the PBL; as noted above, moist convective adjustment does not penetrate |
| Betts-Miller | *Betts* [1986], *Betts and Miller* [1986], M. Miller (personal communication, 1996) | multiple; the Betts-Miller scheme relaxes to a virtual moist adiabat for deep convection originating from the PBL, but it also considers "midlevel convection," in that if buoyancy is found over several layers, the scheme relaxes to a moist adiabat for these layers only with no connection to the PBL |
| Tiedtke | *Tiedtke* [1989] | condensation level for surface air only |
| UKMO | *Gregory and Rowntree* [1990] | anywhere; convection does penetrate; cloud tops can be anywhere |
| Emanuel | *Emanuel* [1991] | anywhere; convection does penetrate |
| Grell | *Grell et al.* [1991] | PBL only |
| Relaxed Arakawa-Schubert | *Moorthi and Suarez* [1992] | PBL only |
| GISS | *Del Genio and Yao* [1993], A. Del Genio (personal communication, 1996) | anywhere, but cloud-base levels are checked sequentially (rather than simultaneously) starting from the lowest level; convection does penetrate; two cloud types are allowed per cloud-base level |
| Hack | *Hack* [1994] | anywhere; convection couples together triplets of layers, so it is "slightly penetrating" |
| Zhang-McFarlane | *Zhang and McFarlane* [1995], G. J. Zhang (personal communication, 1996) | PBL only |

Here $\eta(z, \lambda)$ is the subensemble mass flux, normalized so that it is equal to 1 at the cloud-base level. AS used $\lambda$ to characterize a cloud type, or "subensemble." They assumed that $\lambda$ is independent of height for each subensemble and that detrainment occurs only at the cloud-top level. With these assumptions we can use (1) to determine $\eta(z, \lambda)$, i.e., to find the normalized mass flux as a function of height, up to the cloud-top level, for a given value of $\lambda$:

$$\eta(z, \lambda) = e^{\lambda(z - z_B)} \qquad \text{for } z_B \le z \le z_D(\lambda), \tag{2}$$

where $z_D(\lambda)$ is the detrainment level of the subensemble which has $\lambda$ as its fractional rate of entrainment. Of course,

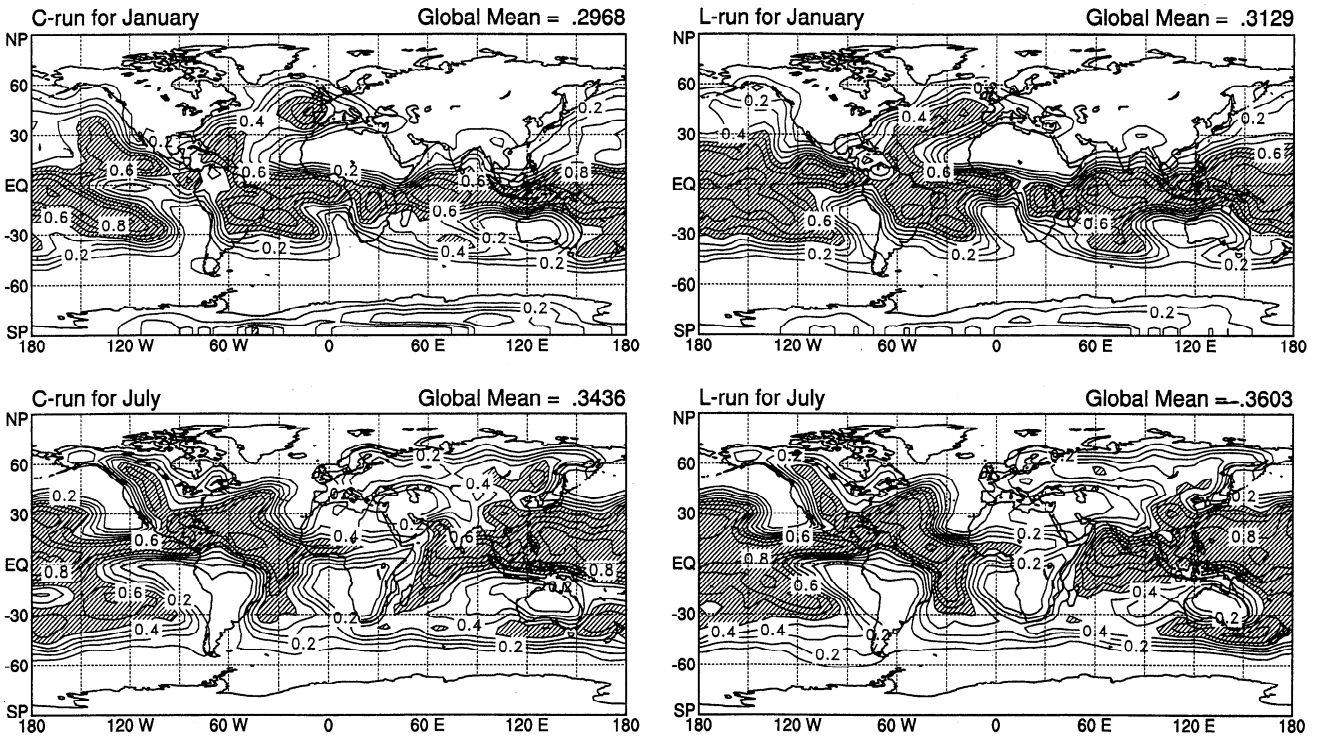


**Figure 2.** January and July cumulus incidence maps from the C run and the L run. The contour interval is 0.1, and values larger than 0.5 are shaded.

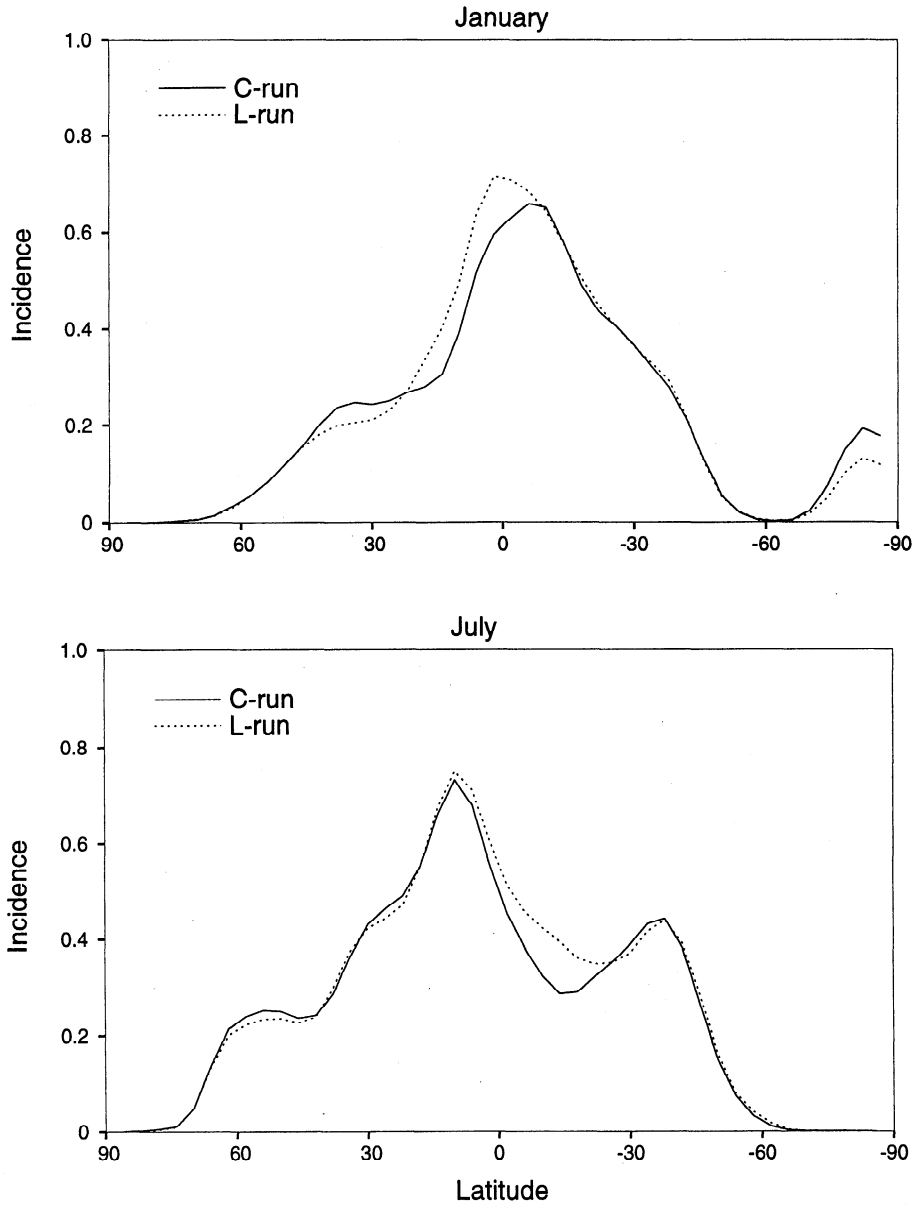


**Figure 3.** Zonally averaged cumulus incidence distributions from the C run (solid line) and the L run (dotted line) for January and July.

$$\eta(z, \lambda) = 0 \qquad \text{for } z > z_D(\lambda), \tag{3}$$

that is, the mass flux is zero above the detrainment level. Corresponding to (1), the moist static energy budget of the cloud satisfies

$$\frac{\partial[\eta(z, \lambda)h_c(z, \lambda)]}{\partial z} = \lambda\eta(z, \lambda)\bar{h}(z) \tag{4}$$

up to the cloud-top level. Here the overbar denotes a large-scale average.

If we neglect virtual temperature effects for simplicity virtual temperature effects are included in the actual implementation described later and are discussed by *Ding* [1995]), the cloud-top neutral buoyancy condition for the subensemble with fractional entrainment rate $\lambda$ and detraining at height $z_D(\lambda)$ is given by

$$h_c[z_D(\lambda), \lambda] = \bar{h}^*[z_D(\lambda)]. \tag{5}$$

If $z_D$ is given, then (5) can be solved as an implicit equation for $\lambda$. Because the mass flux varies exponentially with height, (5) is nonlinear in $\lambda$, and so, as explained by *Lord et al.* [1982], an iterative approach has to be used to solve for $\lambda$. The iteration is complicated and computationally expensive and can be badly behaved for some environmental soundings.

To avoid these difficulties, we assume, following *Moorthi and Suarez* [1992], that the convective mass flux increases linearly with height for each subensemble; that is,

$$\frac{\partial\eta(z, \lambda)}{\partial z} = \lambda, \tag{6}$$

where $\lambda$ is now emphasized as the actual entrainment rate per unit cloud-base mass flux, rather than the fractional entrainment rate, and is assumed to be independent of height for each subensemble. With this approach, the in-cloud moist static energy satisfies

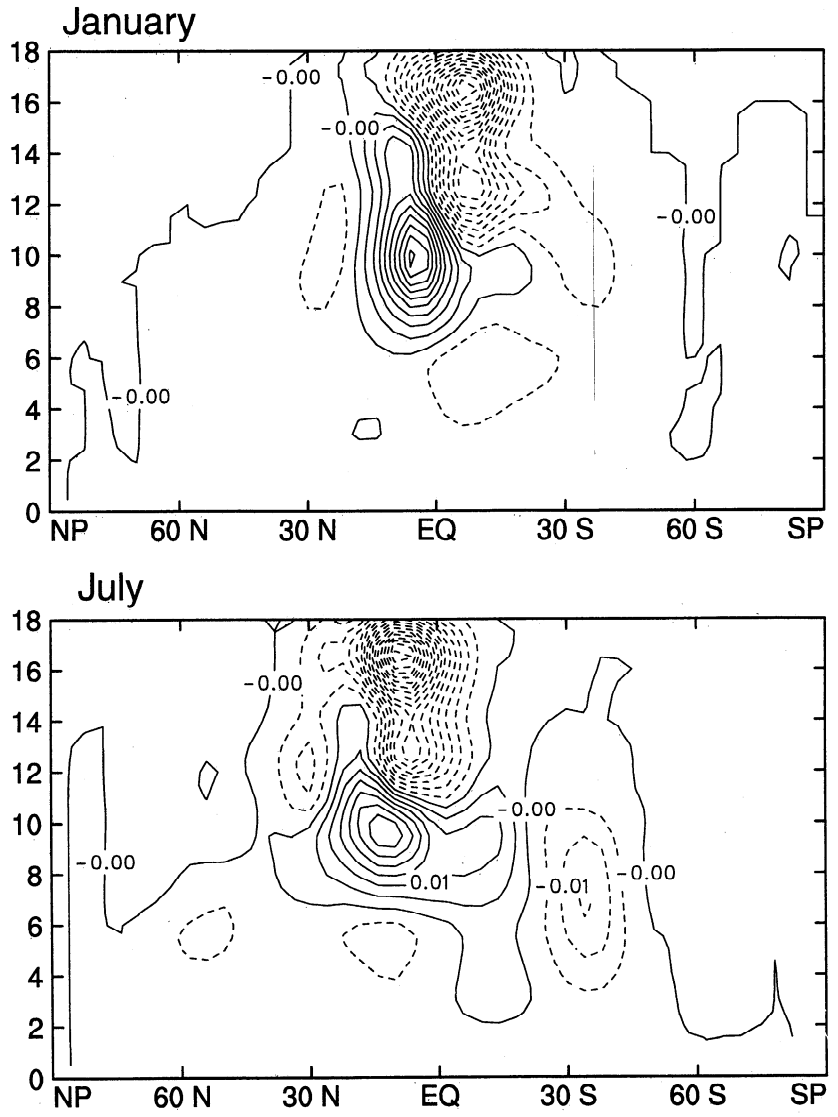


**Figure 4.** Zonally averaged cumulus detrainment mass flux differences between the L run and the C run for (top) January and (bottom) July. The contour interval is 0.005 day$^{-1}$.

$$\frac{\partial[\eta(z, \lambda)h_c(z, \lambda)]}{\partial z} = \lambda \bar{h}(z). \tag{7}$$

By integrating (7) and using (6), we find that the vertical profile of $h_c(z, \lambda)$ satisfies

$$h_c(z, \lambda) = \frac{(h_c)_B + \lambda \int_{z_B}^{z} \bar{h}\, dz}{1 + \lambda(z - z_B)}, \tag{8}$$

where $(h_c)_B$ is the cloud-base value of the updraft moist static energy. As shown by *Ding* [1995], the in-cloud moisture sounding satisfies a similarly simple equation.

With the use of (8) the cloud-top neutral buoyancy condition, (5), can be expressed as

$$(h_c)_B + \lambda \int_{z_B}^{z_D(\lambda)} \bar{h}\, dz = \bar{h}^*[z_D(\lambda)]\{1 + \lambda[z_D(\lambda) - z_B]\}. \tag{9}$$

When $z_D(\lambda)$ is specified, we can solve (9) as a simple linear equation for $\lambda$. This means that we can determine the $\lambda$ needed to ensure neutral buoyancy for a cloud detraining in each model layer. This is how $\lambda$ is determined in the model. *Ding* [1995] shows that a linear equation similar to (9) results when both virtual temperature effects and ice effects are included.

The exponential mass flux profile has no strong physical basis, although the recent work of *Lin and Arakawa* [1997a, b] does provide some support for it. *Moorthi and Suarez* [1992] pointed out that if the cloud-top mass flux is assumed to be the same with the exponential and linear mass flux profiles, then the linear profile will give a larger mass flux in the lower portion of the cloud layer. To partially compensate for this, we have included additional entrainment at the ultimate cloud-top height, following a suggestion of *Cheng and Arakawa* [1993]. With the linear mass flux assumption the normalized cloud-top mass flux can be written as

$$\eta(z_T, \lambda) = 1 + \lambda(z_T - z_B). \tag{10}$$

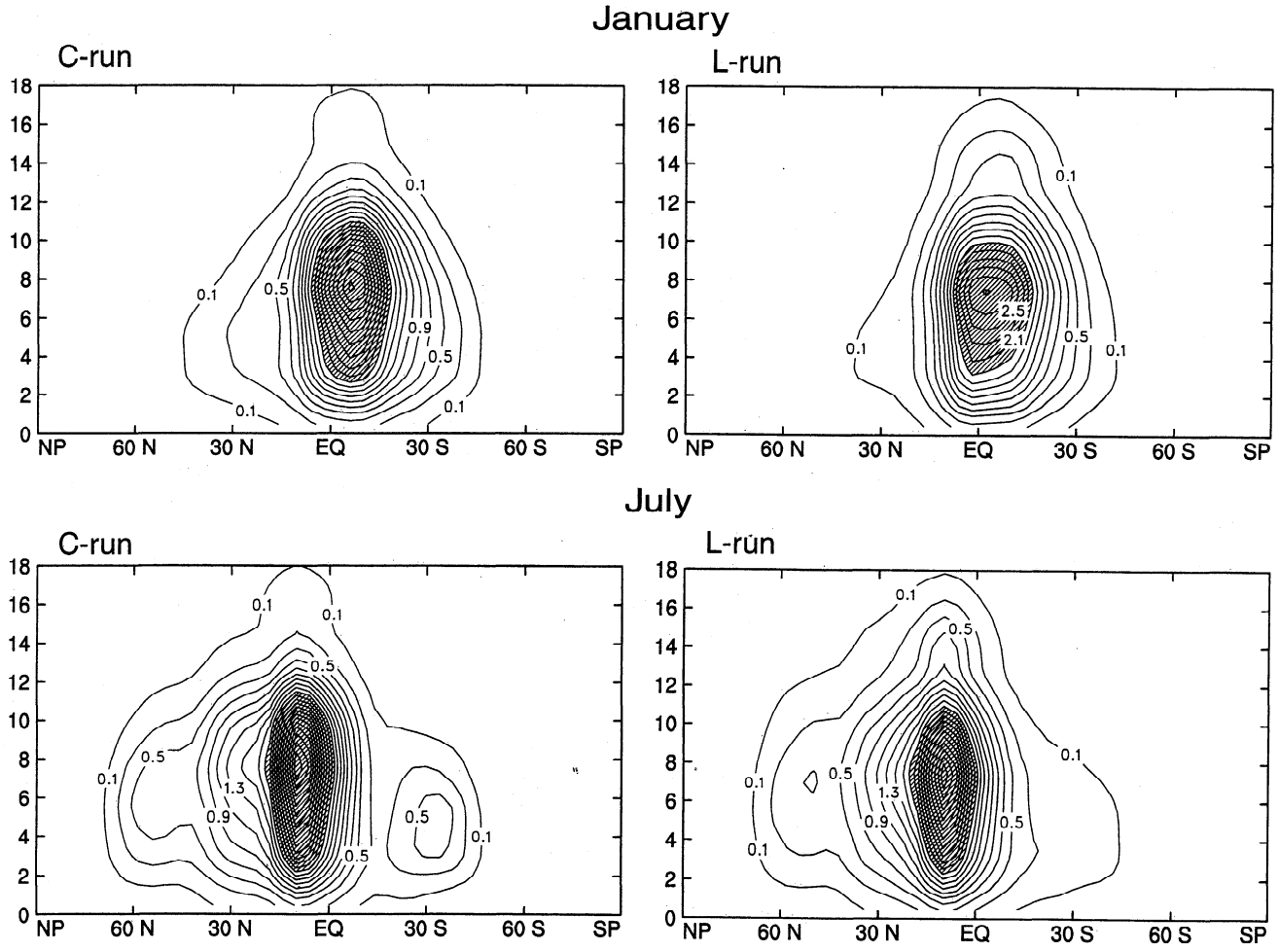


**Figure 5.** January and July zonally averaged cumulus heating rates from the C run and the L run. The contour interval is 0.2 K $d^{-1}$, and values larger than 2 K $d^{-1}$ are shaded.

With cloud-top entrainment, (10) is modified to

$$\eta(z_T, \lambda) = 1 + \lambda(z_T - z_B) + (\Delta\eta)_T, \tag{11}$$

where $(\Delta\eta)_T$ represents the entrainment at the cloud top. *Arakawa and Cheng* [1993] introduced a ratio $\nu$ to measure the amount of cloud-top entrainment; that is,

$$(\Delta\eta)_T = \nu\lambda(z_T - z_B). \tag{12}$$

They found that $\nu = 1$ is a good choice, and we have adopted this value in our study. When we use (11), i.e., the linear mass flux profile with cloud-top entrainment, the mass flux increases rapidly (in fact discontinuously) upward at the cloud top, crudely mimicking the exponential mass flux profile.

All clouds are required to satisfy the following criteria:

1. The entrainment rate must be greater than or equal to zero. When a negative entrainment rate is obtained, the corresponding cloud type is eliminated immediately.
2. The entrainment rate must be smaller than a prescribed maximum value, which is $1.5 \times 10^{-3}$ $m^{-1}$ in our simulations. This value is based on the study of *Sloss* [1967].
3. The $\lambda$ values of clouds with higher cloud-top heights must be smaller than the $\lambda$ values of clouds with lower cloud-top heights [*Nitta*, 1975] so that $\lambda$ decreases with increasing cloud-top height. Because larger $\lambda$ means more entrained environmental air, this will dilute the cloud and cause it to reach neutral buoyancy at a lower level. When this criterion is violated (i.e., when clouds with larger $\lambda$ values have higher cloud-top heights than clouds with smaller $\lambda$ values), the higher clouds are eliminated.
4. The air in the cloud must be saturated at the cloud-top level.
5. The cloud work function must be positive.

The discrete version of the parameterization closely follows *Lord et al.* [1982]; the details of our implementation are discussed by *Ding* [1995].

## 3. Multiple Cloud-Base Levels

When multiple cloud bases are allowed, the cloud-base level becomes a second "cloud-type" index, in addition to the cloud-top index related to $\lambda$. We calculate $\lambda$ for all pairs of cloud-top and cloud-base levels. The calculations of the in-cloud moist static energy budget and in-cloud moisture budget are generalized accordingly in a straightforward manner [*Ding*, 1995].

Consider a model with $N$ layers. If all updrafts start in the PBL, as assumed by AS, then $N - 1$ updraft types exist. If updrafts are permitted to start anywhere and everywhere, however, then there are altogether $\frac{1}{2}N(N - 1)$ possible updrafts, considering all combinations of cloud-base and cloud-top levels. In other words, the introduction of multiple cloud-base

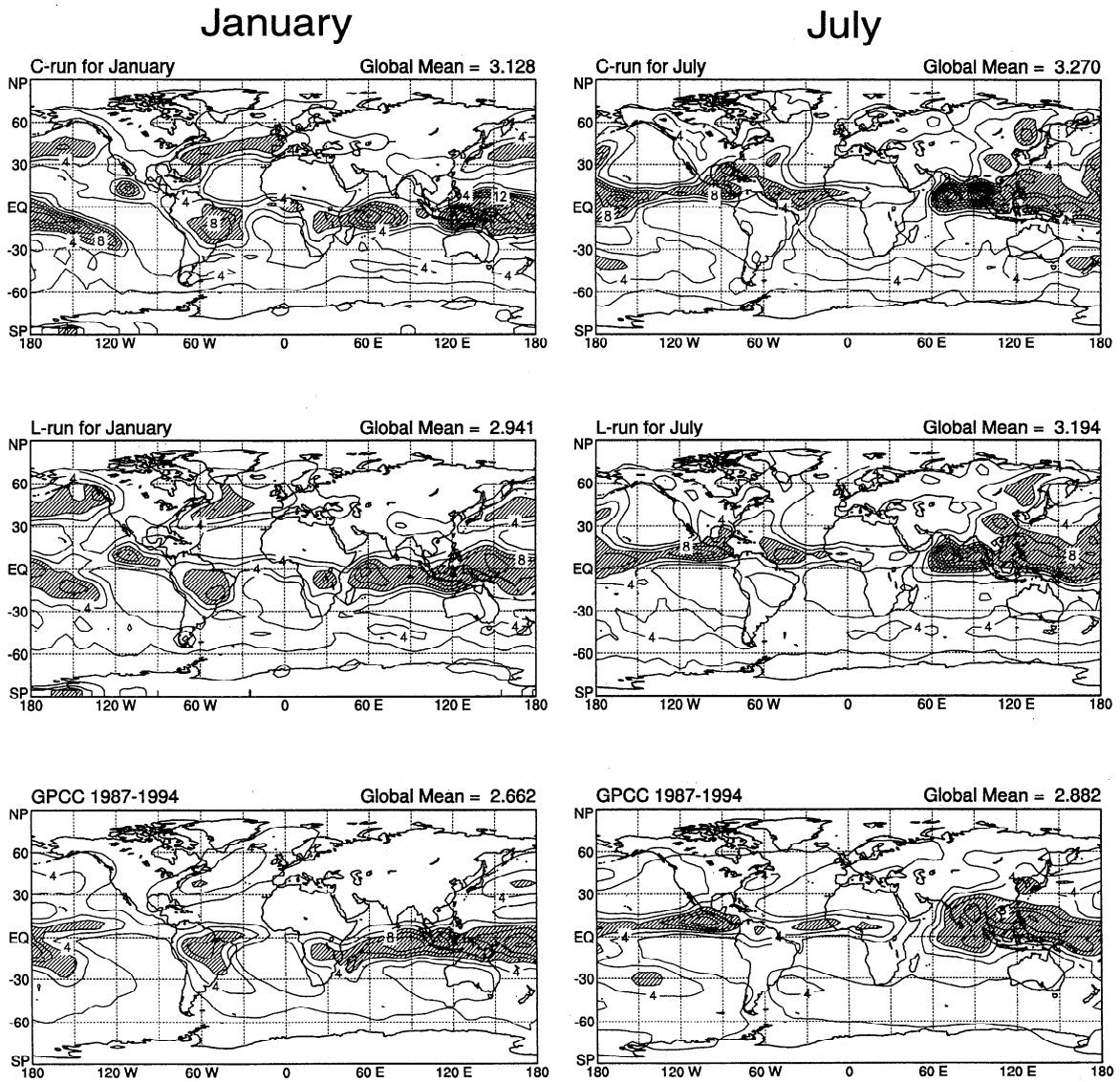


**Figure 6.** January and July total precipitation rate maps from the C run, the L run, and the GPCC observations. The contour interval is 1 mm $d^{-1}$. Shading denotes values larger than 6 mm $d^{-1}$.

levels makes the total number of cloud types increase quadratically with the number of model levels, rather than linearly. Of course, in a global model, only a tiny fraction of the possible updrafts are actually active at any particular time. Nevertheless, it is clear that our approach will become impractical if the vertical resolution of the model becomes very high. Our experience is that for a model with 17 levels the computational requirements are quite acceptable.

## 4. Model Description

In sections 5 and 6, we present the results of numerical experiments using the Colorado State University (CSU) general circulation model (GCM). The control run, referred to below as the C run, uses a version of the GCM that employs the prognostic convective closure described by *Randall and Pan* [1993] and *Pan and Randall* [1997], the stratiform cloud microphysics paramcterization developed by *Fowler et al.* [1996] and *Fowler and Randall* [1996a, b], and the land-surface parameterization developed by *Sellers et al.* [1996a, b] and tested by *Randall et al.* [1996]. For detailed descriptions of the model and its performance, see the papers cited above, and also *Randall et al.* [1991].

## 5. Tests of Linear Convective Mass Flux in a GCM

The annual-cycle C run started from a June 1 initial condition obtained from an earlier multiyear run of the GCM. A similar annual cycle run, called the L run, was carried out using the linear mass flux profile but with no other changes. MSTADJ was used to represent convection originating above the PBL in both the C run and the L run.

Figure 2 shows maps of the January and July cumulus incidence (i.e., frequency of occurrence) for the C and L runs. The corresponding zonal means are shown in Figure 3. In these figures, "cumulus incidence" does not include the incidence of MSTADJ. The two versions of the model generate very similar cumulus incidence patterns. The global mean cumulus incidence of the L run is larger than that of the C run for both

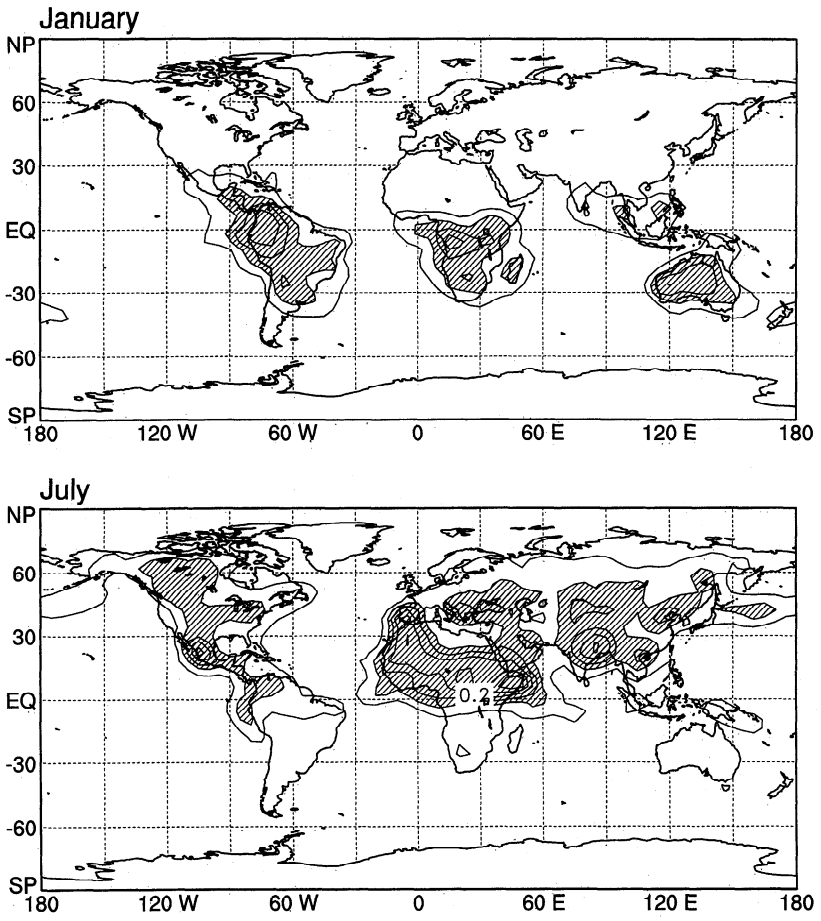


**Figure 7.** Differences between the total cumulus incidence and the incidence of cumulus clouds starting from the PBL for the MCB run. The contour interval is 0.05. Values larger than 0.1 are shaded.

seasons. In the tropics the largest values of the cumulus incidence exceed 80%, as would be expected for such large grid boxes.

Figure 4 shows the zonally averaged cumulus detrainment mass flux differences between the L run and the C run for (top) January and (bottom) July. Relative to the C run, the L run produces less cumulus detrainment in the upper tropical troposphere but more in the middle tropical troposphere for both January and July. The convective activity has thus generally shifted downward. Figure 5 shows the corresponding results for the January and July zonally averaged cumulus heating rates in the two runs. The maximum heating in the L run is smaller than that in the C run for both January and July. Unfortunately, we cannot compare these heating rates with observations, because none are available. The level of maximum heating is essentially the same in the two versions of the model for both seasons.

The simulated and observed January and July total precipitation rate maps are shown in Figure 6. The L run produces less total precipitation than the C run for both January and July, and this is due to a reduction of the cumulus precipitation rate. These changes are consistent with the reduced convective heating discussed above. The total precipitation rates of the L run agree better with observations than those of the C run. For example, the January maximum value is 12.0 mm $d^{-1}$ in the L run and 19.0 mm $d^{-1}$ in the C run. The observed January maximum is 12.4 mm $d^{-1}$ according to the data of the Global Precipitation Climatology Project (GPCP) [*Xie and Arkin*, 1996]. For July the maximum of the L run, 19.0 mm $d^{-1}$, is larger than the GPCP-observed maximum of 13.9 mm $d^{-1}$, but both are much smaller than the C-run maximum of 26.3 mm $d^{-1}$. The global mean values of the L run are in better agreement with observations than those of the C run. The water vapor, temperature, and wind distributions produced by the two runs are quite similar and so are not shown here.

The L run saves about 70% of the computing time used by the cumulus parameterization, compared with the C run. The prognostic closure introduced by *Pan and Randall* [1997] and used here reduces the computing requirements of the cumulus parameterization by about a factor of 2, relative to the version with the quasi-equilibrium closure [*Lord et al.*, 1982]. This means that the cumulus parameterization used in the L run consumes about one sixth of the computing time used by the original version of the cumulus parameterization with the quasi-equilibrium closure and the exponential mass flux profile. Obviously, a savings of this magnitude is of considerable practical importance.

In summary, the linear mass flux version of the model produces smoother distributions of precipitation and convective heating, with weaker maxima. The cumulus detrainment mass flux profile shifts downward in the tropics. Despite these changes in the convective activity, the linear mass flux and exponential mass flux produce very similar distributions of the thermodynamic and wind fields. The linear mass flux assump-

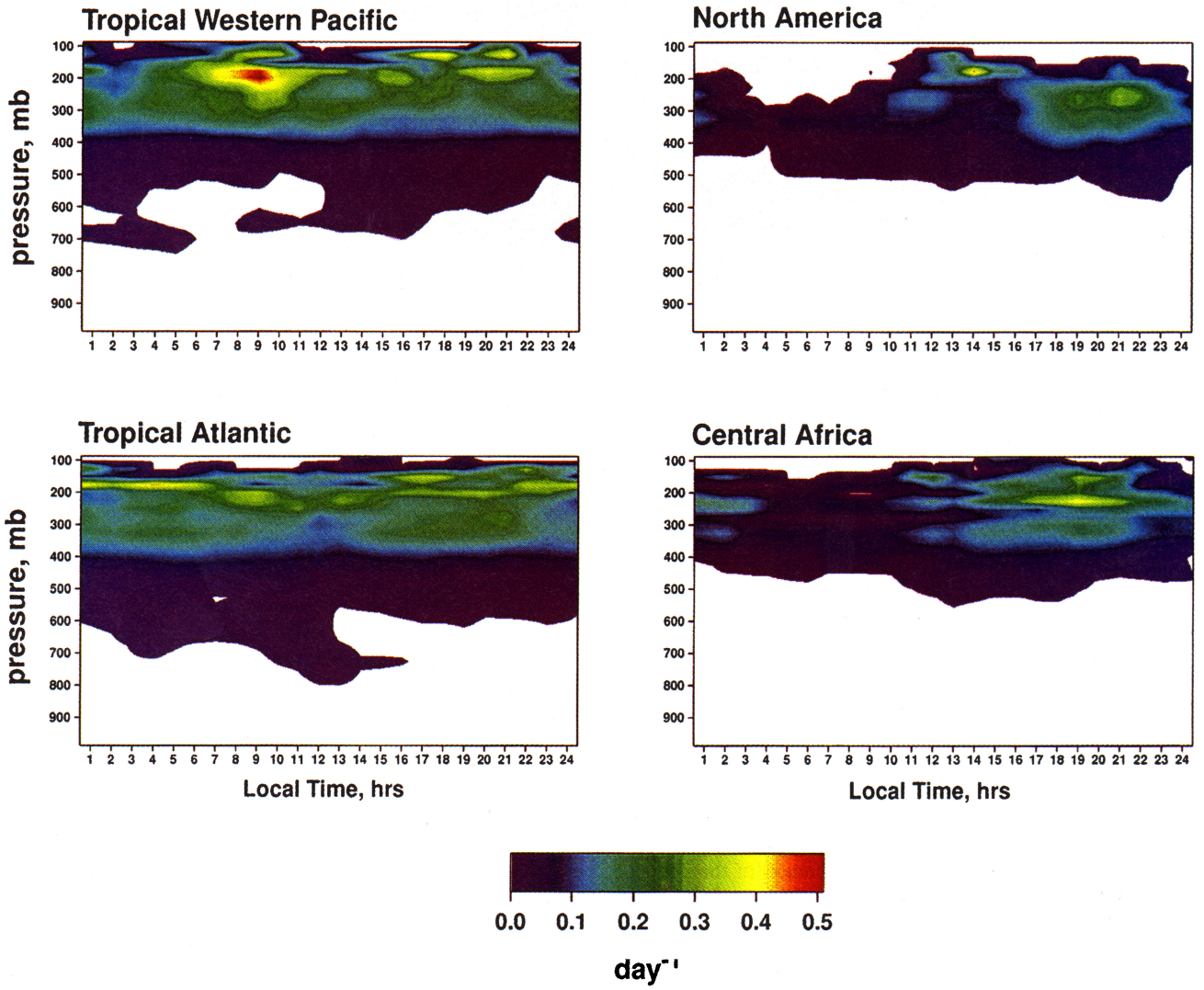


**Plate 1.** Diurnal changes of the cumulus detrainment mass flux for the tropical western Pacific Ocean, North America, the tropical Atlantic Ocean, and central Africa. The units are days$^{-1}$. Here the timescale is that required for replacement of the air in the grid cell by newly detrained air.

tion reduces the computational cost of the parameterization by 70%, relative to a version with the exponential mass flux, when both versions use the prognostic closure.

## 6. Effects of Multiple Cloud-Base Levels

We now present the results of an annual cycle run with multiple cloud-base levels, in which the MSTADJ parameterization was disabled; this is referred to below as the MCB run. The MCB run can be directly compared with the L run, because both use the linear mass flux profile for each cloud type. We also make some comparisons between the MCB run and the C run.

Although the L run and the MCB run produce similar patterns of cumulus activity, the globally averaged cumulus incidence increases in the MCB simulation in both January and July. This is to be expected, simply because there are many more potential cloud types in the MCB run. The cumulus incidence distributions from the two runs are qualitatively quite similar. Figure 7 shows the differences between the total cumulus incidence and the incidence of cumulus clouds starting from the PBL for the MCB run. A plot of the difference between the total cumulus incidence in the MCB run and the L run would look almost the same. The figure makes it clear that COA activity occurs mainly over the summer and tropical continents. Why should this be so? What is "special" about convection over the continents? One important factor is that continental convection is strongly modulated by the diurnal cycle, much more so than oceanic convection. In addition, the continental boundary layer undergoes a very pronounced cycle of diurnal deepening and shallowing [e.g., *Randall et al.*, 1985]. As the continental planetary boundary layer (PBL) becomes shallower in response to the early-evening cooling of the surface, the air that has been inside the PBL, which may have been considerably warmed and moistened by the surface fluxes during the preceding daylight hours, is left behind and becomes part of the free atmosphere. This warm, humid air in the free atmosphere can then serve as a source layer or cloud-base layer for moist convection, either during the nighttime hours or on the following day. In short, the diurnal cycle of the continental PBL "pumps" warm, moist air into the free atmosphere,

**Table 2.** A Measure of the Cumulus Incidence for Each Cloud Type in the MCB Run

| Base Level | Top Level 16 | 15 | 14 | 13 | 12 | 11 | 10 | 9 | 8 | 7 | 6 | 5 | 4 | 3 |
|---|---|---|---|---|---|---|---|---|---|---|---|---|---|---|
| 4 | ... | ... | ... | ... | ... | ... | ... | ... | ... | ... | ... | ... | ... | 10.7 |
| 5 | ... | ... | ... | ... | ... | ... | ... | ... | ... | ... | ... | ... | 17.7 | 1.81 |
| 6 | ... | ... | ... | ... | ... | ... | ... | ... | ... | ... | ... | 15.0 | 1.74 | 1.74 |
| 7 | ... | ... | ... | ... | ... | ... | ... | ... | ... | ... | 4.75 | 1.20 | 1.87 | 0.44 |
| 8 | ... | ... | ... | ... | ... | ... | ... | ... | ... | 2.31 | 1.27 | 0.42 | 0.44 | 0.14 |
| 9 | ... | ... | ... | ... | ... | ... | ... | ... | 1.32 | 0.15 | 0.41 | 0.23 | 0.18 | 0.02 |
| 10 | ... | ... | ... | ... | ... | ... | ... | 1.01 | 0.16 | 0.28 | 0.16 | 0.10 | 0.04 | 0.01 |
| 11 | ... | ... | ... | ... | ... | ... | 0.51 | 0.18 | 0.34 | 0.12 | 0.05 | 0.03 | 0.02 | 0.01 |
| 12 | ... | ... | ... | ... | ... | 0.26 | 0.68 | 0.99 | 0.33 | 0.13 | 0.04 | 0.03 | 0.02 | 0.01 |
| 13 | ... | ... | ... | ... | 0.03 | 2.23 | 3.44 | 1.28 | 0.49 | 0.18 | 0.05 | 0.04 | 0.03 | 0.01 |
| 14 | ... | ... | ... | 0.23 | 5.62 | 12.7 | 8.18 | 3.65 | 1.49 | 0.64 | 0.25 | 0.19 | 0.12 | 0.05 |
| 15 | ... | ... | 0.6 | 8.93 | 25.8 | 23.0 | 14.8 | 8.02 | 3.89 | 1.95 | 1.12 | 0.78 | 0.63 | 0.30 |
| 16 | ... | 1.35 | 10.3 | 34.5 | 45.9 | 43.8 | 31.8 | 19.8 | 11.5 | 6.79 | 3.87 | 3.20 | 2.12 | 1.30 |
| 17 | 38.9 | 300.2 | 156.1 | 169.3 | 201.3 | 241.8 | 234.4 | 172.0 | 116.2 | 72.8 | 45.0 | 40.7 | 32.8 | 17.3 |

Larger values indicate more frequent occurrence; only the relative values are meaningful. The different rows correspond to different cloud-base levels, and the different columns correspond to different cloud-top levels. These results were produced with a 17-layer model. Level 4 corresponds to roughly the 150 mbar level.

where it can act as a source layer for convection at a later time. In contrast, the diurnal cycle of the oceanic PBL is quite weak. The diurnal PBL pump would thus be expected to promote COA over the continents but not over the oceans. This is a possible explanation for the results shown in Figure 7.

To investigate these ideas, we chose two representative continental locations and two ocean locations and examined the diurnal changes of the cumulus activity in the July MCB simulation. The locations chosen are the tropical western Pacific Ocean, North America, the tropical Atlantic Ocean, and central Africa. Plate 1 shows the diurnal changes of the cumulus detrainment mass flux for these four locations. Over the western Pacific Ocean, deep cumulus activity has an early morning maximum, consistent with the results of *Randall et al.* [1991]. The diurnal changes over the tropical Atlantic Ocean are weaker, but there is still some tendency for a nocturnal maximum. For the two continental locations the most vigorous cumulus activity occurs in the late afternoon and early evening, and there is a minimum in the early morning.

We remark that the relatively large values of the cumulus incidence over the Sahara Desert, which can be seen in the July MCB results shown in the bottom panel of Figure 7, do not correspond to large precipitation amounts at the surface.

In order to analyze the cumulus cloud-type distribution in more detail, we kept track of cumulus incidence and cloud-base mass fluxes in the MCB run, for all cloud types and all grid points, for July only. The results are shown in Tables 2 and 3, respectively. Cumulus clouds starting in the PBL dominate, but there are many cumulus clouds originating in the free atmosphere. Table 2 shows that most cumulus clouds with high tops start from the PBL and other relatively low levels. For example, most cumulus clouds with tops at levels 4 and 3 have bases at levels 17 and 16. Frequently occurring clouds include those with tops at level 3 and bases at level 4 and those with tops at level 4 and bases at level 5. These high-level but shallow convective clouds occur mainly in the western Pacific, southern Asia, the tropical Atlantic, and the tropical eastern Pacific. Except in southern Asia, most of them do not occur together with deep convective clouds. They might be interpreted as cirrocumulus clouds. The most active cumulus clouds in the model, as measured by incidence, are shallow, low-level clouds with tops at level 15 and bases in the PBL. Clouds with bases

**Table 3.** As in Table 2 But for the Cumulus Cloud-Base Mass Flux

| Base Level | Top Level 16 | 15 | 14 | 13 | 12 | 11 | 10 | 9 | 8 | 7 | 6 | 5 | 4 | 3 |
|---|---|---|---|---|---|---|---|---|---|---|---|---|---|---|
| 4 | ... | ... | ... | ... | ... | ... | ... | ... | ... | ... | ... | ... | ... | 1.01 |
| 5 | ... | ... | ... | ... | ... | ... | ... | ... | ... | ... | ... | ... | 1.12 | 0.24 |
| 6 | ... | ... | ... | ... | ... | ... | ... | ... | ... | ... | ... | 0.98 | 0.04 | 0.04 |
| 7 | ... | ... | ... | ... | ... | ... | ... | ... | ... | ... | 0.26 | 0.03 | 0.04 | 0.04 |
| 8 | ... | ... | ... | ... | ... | ... | ... | ... | ... | 0.12 | 0.01 | 0.01 | 0.01 | 0.01 |
| 9 | ... | ... | ... | ... | ... | ... | ... | ... | 0.12 | 0.00 | 0.01 | 0.01 | 0.01 | 0.01 |
| 10 | ... | ... | ... | ... | ... | ... | ... | 0.09 | 0.0 | 0.01 | 0.01 | 0.0 | 0.0 | 0.0 |
| 11 | ... | ... | ... | ... | ... | ... | 0.03 | 0.0 | 0.01 | 0.0 | 0.0 | 0.0 | 0.0 | 0.0 |
| 12 | ... | ... | ... | ... | ... | 0.0 | 0.02 | 0.03 | 0.01 | 0.01 | 0.0 | 0.0 | 0.0 | 0.0 |
| 13 | ... | ... | ... | ... | 0.0 | 0.05 | 0.11 | 0.06 | 0.03 | 0.02 | 0.01 | 0.01 | 0.01 | 0.0 |
| 14 | ... | ... | ... | 0.0 | 0.13 | 0.53 | 0.61 | 0.39 | 0.21 | 0.12 | 0.04 | 0.04 | 0.03 | 0.01 |
| 15 | ... | ... | 0.01 | 0.22 | 1.25 | 1.95 | 1.84 | 1.34 | 0.79 | 0.45 | 0.26 | 0.19 | 0.19 | 0.09 |
| 16 | ... | 0.10 | 0.23 | 1.67 | 4.07 | 5.57 | 5.47 | 4.55 | 3.05 | 1.86 | 1.04 | 0.95 | 0.57 | 0.32 |
| 17 | 0.95 | 13.5 | 11.9 | 16.8 | 25.9 | 42.4 | 56.9 | 54.2 | 43.1 | 29.5 | 18.7 | 19.4 | 17.9 | 8.33 |

In units of $10^{-2}$ kg m$^{-2}$ h$^{-1}$.

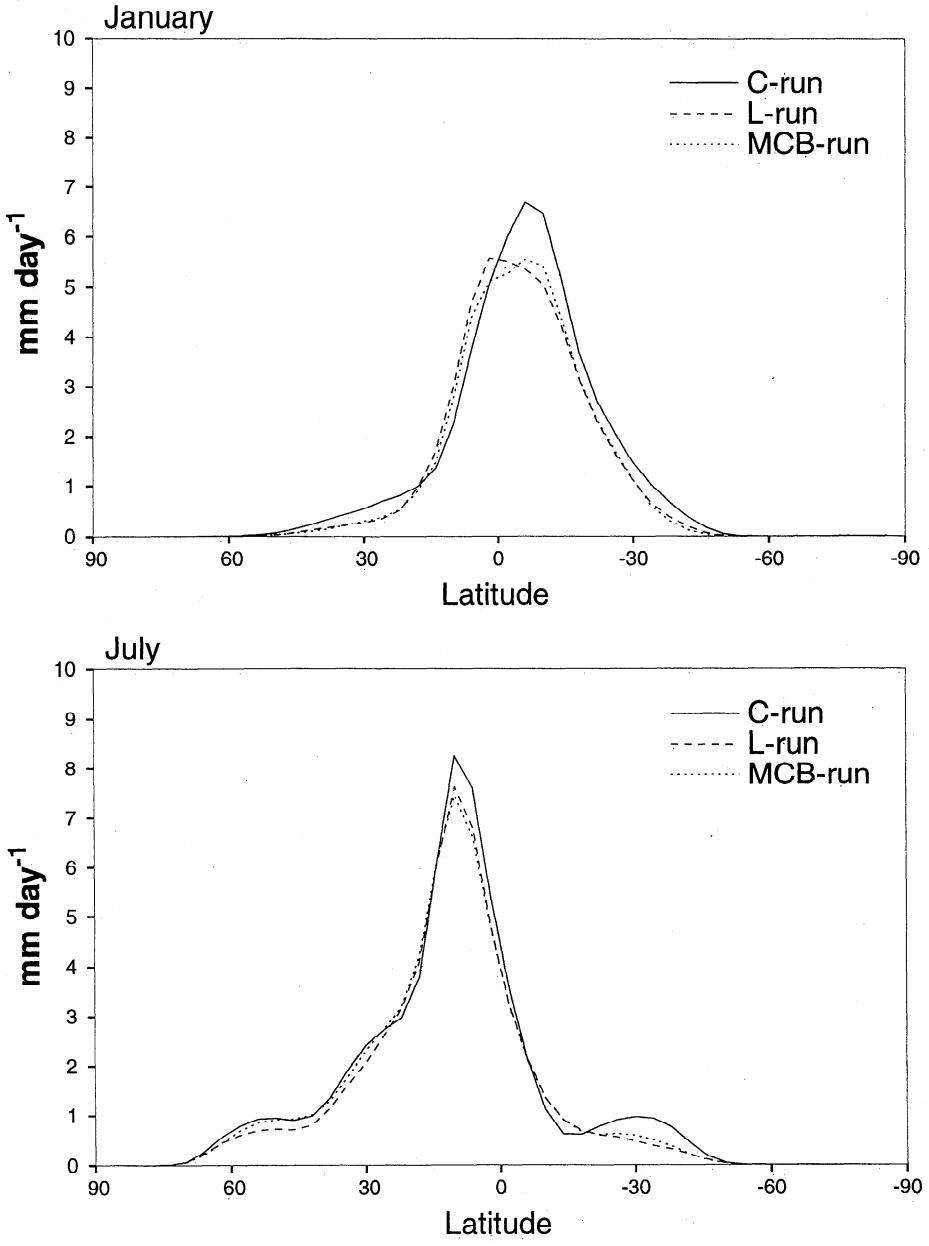


**Figure 8.** Zonally averaged cumulus precipitation rates from the C run, the L run, and the MCB run.

in the PBL and tops at levels 9, 10, and 11 are also very active. Tables 2 and 3 together show that many COA have their bases at relatively low levels, close to the PBL. This is consistent with the earlier discussion, which suggested that an important mechanism for generation of COA is the diurnal cycle of the PBL over the summer and tropical continents.

In the C and L runs, MSTADJ represents nonpenetrative COA, i.e., clouds that couple only neighboring model layers. Table 2 shows that in the MCB run, most such nonpenetrative clouds occur in the upper troposphere. Overall, these one-layer clouds make up only a small fraction of the COA. This shows that we cannot fully represent the effects of COA by using MSTADJ. As shown in Table 3, the nonpenetrative COA contribute even less as measured by their mass flux.

Further analysis shows that PBL-rooted and elevated convection occur together at the same grid point on the same time step primarily when an "anvil" cloud exists at the top of deep convection.

As would be expected, the changes of the simulated total precipitation rate in the MCB run, relative to the C run, are mainly due to changes in the simulated cumulus precipitation rate. The zonally averaged cumulus precipitation rates obtained in the C run, the L run, and the MCB run are shown in Figure 8. The curves for the L run resemble those of the MCB run, and both are quite different from those of the C run. The simulated total precipitation rate consists of the sum of large-scale precipitation [*Fowler et al.*, 1996] and cumulus precipitation. Overall, the MCB run produces slightly less total precipitation than the C run.

Further analysis of the model results shows that the intensity of deep tropical cumulus convection, as measured by the detrainment mass flux and upper tropospheric convective heating

and drying, is reduced with the MCB parameterization and that the level of the highest cloud tops shifts downward. This suggests that cumulus clouds starting from the free atmosphere, as included in the MCB run, tend to retard the development of deep penetrative convection to some degree. An interpretation is that COA competes for the convective available potential energy which would otherwise be available to the convective clouds originating in the PBL. The simulated temperature, humidity, and wind fields produced in the various runs are very similar and so are not shown here.

## 7. Concluding Remarks

Observational and modeling studies suggest that cumulus clouds, including some deep clouds, can originate above the PBL and can be quite active. We have modified the Arakawa-Schubert cumulus parameterization so that it can represent clouds originating simultaneously at any and all levels. The number of potential cloud types increases dramatically. Because this adds complexity, we began by simplifying the parameterization through the introduction of the linear mass flux profile with cloud-top entrainment.

The linear mass flux model leads to a simpler and computationally less expensive algorithm for finding the entrainment rate associated with clouds that lose their buoyancy at particular model levels. The precipitation pattern produced with the linear mass flux is smoother with weaker maxima. The depth of the convective layer decreases slightly. These changes seem to be improvements in the simulated climate of the model. The large-scale dynamical and thermodynamical fields are hardly affected by the change from the exponential to the linear mass flux.

When multiple cloud bases are permitted in the model, the simulated COA tends to occur over land and is associated with the warm moist air pumped into the free atmosphere by the diurnally varying PBL depth. We also find considerable COA activity at upper levels in the tropics, associated with convection in moist layers produced by the detrainment from cumuli that originate in the boundary layer.

As this paper is written, a "typical" GCM has about 20 layers [e.g., *Gates*, 1992]. It appears likely that in the next few years we will see models with 100 or more layers. Clearly, any physical parameterization that has computing requirements which scale quadratically with the number of model layers is going to become prohibitively expensive for use in such models. This applies to the convection parameterization described here and also to some longwave radiation parameterizations, and even to some turbulence parameterizations. As discussed, for example, by *Stull* [1984], eddy mass transport across finite distances is the norm in nature; this applies to both boundary layer turbulence and cumulus convection. We must try to formulate these parameterizations so that they can represent the essential physics but still scale only linearly with the number of model layers. This is an interesting challenge for the future.

**Acknowledgments.** D. Dazlich of CSU provided valuable assistance with the GCM. This research has been supported by the National Science Foundation under grant ATM-9214981, by the Department of Energy under grant DE-FG-03-94ER61929, and by subcontract 0965-G-5B387 from UCLA. Computing resources were provided by the National Energy Research Computer Center at the Lawrence Livermore National Laboratory.

## References

Anthes, R. A., A cumulus parameterization scheme utilizing a one-dimensional cloud model, *Mon. Weather Rev.*, *105*, 270–286, 1977.

Arakawa, A., and M.-D. Cheng, The Arakawa-Schubert cumulus parameterization, in *The Representation of Cumulus Convection in Numerical Models of the Atmosphere*, edited by K. A. Emanuel and D. J. Raymond, *Meteorol. Monogr.*, *24*(46), 123–136, 1993.

Arakawa, A., and W. H. Schubert, The interaction of a cumulus cloud ensemble with the large-scale environment, I, *J. Atmos. Sci.*, *31*, 674–701, 1974.

Betts, A. K., A new convective adjustment scheme, I, Observational and theoretical basis, *Q. J. R. Meteorol. Soc.*, *112*, 677–691, 1986.

Betts, A. K., and M. J. Miller, A new convective adjustment scheme, II, Single column tests using GATE wave, BOMEX, ATEX, and arctic air-mass data sets, *Q. J. R. Meteorol. Soc.*, *112*, 693–709, 1986.

Cheng, M.-D., and A. Arakawa, A cumulus parameterization with rainwater budget and convective downdrafts, in *20th Conference on Hurricanes and Tropical Meteorology*, pp. 313–316, Am. Meteorol. Soc., Boston, Mass., 1993.

Colman, B., A case study of elevated convection in an unsaturated large-scale environment, in *Mesoscale Meteorology—Theories, Observations and Models*, edited by D. K. Lilly and T. Gal-Chen, D. Reidel, Norwell, Mass., 1983.

Del Genio, A. D., and M. S. Yao, Efficient cumulus parameterization for long-term climate studies: The GISS scheme, in *The Representation of Cumulus Convection in Numerical Models*, pp. 181–184, Am. Meteorol. Soc., Boston, Mass., 1993.

Ding, P., A parameterization of cumulus convection with multiple cloud base levels, 235 pp., Ph.D. thesis, Colo. State Univ., Fort Collins, 1995.

Emanuel, K. A., A scheme for representing cumulus convection in large-scale models, *J. Atmos. Sci.*, *48*, 2313–2335, 1991.

Fowler, L. D., and D. A. Randall, Liquid and ice cloud microphysics in the CSU general circulation model, 2, Simulation of the Earth's radiation budget, *J. Clim.*, *9*, 530–560, 1996a.

Fowler, L. D., and D. A. Randall, Liquid and ice cloud microphysics in the CSU general circulation model, 3, Sensitivity tests, *J. Clim.*, *9*, 561–586, 1996b.

Fowler, L. D., D. A. Randall, and S. A. Rutledge, Liquid and ice cloud microphysics in the CSU general circulation model, I, Model description and results of a baseline simulation, *J. Clim.*, *9*, 489–529, 1996.

Gates, W. L., AMIP: The Atmospheric Model Intercomparison Project, *Bull. Am. Meteorol. Soc.*, *73*, 1962–1970, 1992.

Gregory, D., and P. R. Rowntree, A mass flux convection scheme with representation of cloud ensemble characteristics and stability-dependent closure, *Mon. Weather Rev.*, *118*, 1483–1506, 1990.

Grell, G. A., Y.-H. Kuo, and R. J. Pasch, Semi-prognostic tests of cumulus parameterization schemes in the middle latitude, *Mon. Weather Rev.*, *119*, 5–31, 1991.

Hack, J. J., Parameterization of moist convection in the National Center for Atmospheric Research Community Climate Model (CCM2), *J. Geophys. Res.*, *99*, 5551–5568, 1994.

Holle, R. L., J. Simpson, and S. W. Leavitt, GATE B-scale cloudiness from whole-sky cameras on four U.S. ships, *Mon. Weather Rev.*, *107*, 874–895, 1979.

Kuo, H. L., On formation and intensification of tropical cyclones throughout latent heat release by cumulus convection, *J. Atmos. Sci.*, *22*, 40–63, 1965.

Kuo, H.-L., Further studies of the parameterization of the influence of cumulus convection on large-scale flow, *J. Atmos. Sci.*, *31*, 1232–1240, 1974.

Lin, C., and A. Arakawa, The macroscopic entrainment processes of simulated cumulus ensemble, I, Entrainment sources, *J. Atmos. Sci.*, *54*, 1027–1043, 1997a.

Lin, C., and A. Arakawa, The macroscopic entrainment processes of simulated cumulus ensemble, II, Testing the entraining plume model, *J. Atmos. Sci.*, *54*, 1044–1053, 1997b.

Lord, S. J., W. C. Chao, and A. Arakawa, Interaction of a cumulus cloud ensemble with the large-scale environment, IV, The discrete model, *J. Atmos. Sci.*, *39*, 104–113, 1982.

Manabe, S., J. Smagorinsky, and R. F. Strickler, Simulated climatology of a general circulation model with a hydrologic cycle, *Mon. Weather Rev.*, *93*, 769–797, 1965.

Moorthi, S., and M. J. Suarez, Relaxed Arakawa-Schubert: A param-

eterization of moist convection for general circulation models, *Mon. Weather Rev.*, *120*, 978–1002, 1992.

Nitta, T., Observational determination of cloud mass flux distributions, *J. Atmos. Sci.*, *32*, 73–91, 1975.

Pan, D.-M., and D. A. Randall, A prognostic cumulus parameterization, *Q. J. R. Meteorol. Soc.*, in press, 1997.

Randall, D. A., and D.-M. Pan, Implementation of the Arakawa-Schubert cumulus parameterization with a prognostic closure, in *Cumulus Parameterization*, edited by K. Emanuel and D. Raymond, pp. 137–144, Am. Meteorol. Soc., Boston, Mass., 1993.

Randall, D. A., J. A. Abeles, and T. G. Corsetti, Seasonal simulations of the planetary boundary layer and boundary-layer stratocumulus clouds with a general circulation model, *J. Atmos. Sci.*, *42*, 641–676, 1985.

Randall, D. A., Harshvardhan, D. A. Dazlich, and T. G. Corsetti, Interactions among radiation, convection, and large-scale dynamics in a general circulation model, *J. Atmos. Sci.*, *46*, 1943–1970, 1989.

Randall, D. A., Harshvardhan, and D. A. Dazlich, Diurnal variability of the hydrologic cycle in a general circulation model, *J. Atmos. Sci.*, *48*, 40–62, 1991.

Randall, D. A., et al., A revised land-surface parameterization (SiB2) for atmospheric GCMs, 3, The greening of the CSU general circulation model, *J. Clim.*, *9*, 738–763, 1996.

Raymond, D. J., and K. A. Emanuel, The Kuo cumulus parameterization, in *The Representation of Cumulus Convection in Numerical Models*, edited by K. A. Emanuel and D. J. Raymond, *Meteorol. Monogr.*, *24*(46), 145–154, 1993.

Sloss, P. W., An empirical examination of cumulus entrainment, *J. Appl. Meteorol.*, *9*, 878–881, 1967.

Stull, R. B., Transilient turbulence theory, I, The concept of eddy mixing across finite distances, *J. Atmos. Sci.*, *41*, 3351–3367, 1984.

Suarez, M., A. Arakawa, and D. A. Randall, Parameterization of the planetary boundary layer in the UCLA general circulation model: Formulation and results, *Mon. Weather Rev.*, *111*, 2224–2243, 1983.

Tiedtke, M., A comprehensive mass flux scheme for cumulus parameterization in large-scale models, *Mon. Weather Rev.*, *117*, 1779–1800, 1989.

Warner, C., and R. H. Grumm, Cloud distributions in a Bay of Bengal monsoon depression, *Mon. Weather Rev.*, *112*, 153–172, 1984.

Warner, C., J. Simpson, G. Van Helvoirt, D. W. Marth, D. Suchman, and G. L. Austin, Deep convection on Day 261 of GATE, *Mon. Weather Rev.*, *108*, 169–194, 1980.

Xie, P., and P. A. Arkin, Analyses of global monthly precipitation using gauge observations, satellite estimates, and numerical model predictions, *J. Clim.*, in press, 1996.

Zhang, G. J., and N. A. McFarlane, Sensitivity of climate simulations to the parameterization of cumulus convection in the Canadian Climate Centre general circulation model, *Atmos. Ocean*, *33*, 407–446, 1995.

---

P. Ding and D. A. Randall, Department of Atmospheric Science, Colorado State University, Fort Collins, CO 80523. (randall@redfish.atmos.colostate.edu)

(Received December 19, 1996; revised August 5, 1997; accepted January 28, 1998.)